Nonequilibrium quantum criticality of interacting Dirac fermions

Yin-Kai Yu[1], Zhi Zeng[1], Zi-Xiang Li[2,✉], and Shuai Yin[1,✉]

[1]School of physics, Sun Yat-Sen University, Guangzhou 510275, China
[2]Beijing National Laboratory for Condensed Matter Physics & Institute of Physics, Chinese Academy of Sciences, Beijing 100190, China
✉e-mail: zixiangli@iphy.ac.cn
✉e-mail: yinsh6@mail.sysu.edu.cn

The interaction of Dirac fermions in condensed matter systems can result in phase transitions that go beyond the Landau paradigm, presenting both high theoretical value and challenges. However, the non-equilibrium criticality problem has not yet been reliably studied numerically. In this study, we use determinant quantum Monte Carlo to demonstrate the relaxation dynamics of Dirac fermions for the first time. Specifically, we investigate the honeycomb Hubbard model by simulating short-imaginary-time evolution behavior at critical points for antiferromagnetic initial states, Dirac semimetal initial states, and spin random up-down initial states. Through our calculations, we determine the controversial critical point and critical exponents in this model and establish an initial slip exponents $\theta = -0.84(4)$ for chiral Heisenberg universality class — a first-time achievement. Our method fully utilizes short-time information before reaching equilibrium state which improves efficiency of quantum Monte Carlo simulations significantly. This approach opens up new avenues for numerical studies on non-equilibrium fermion criticality that can be universally applied to other cases. The potential for nonequilibrium fermion Monte Carlo in addressing the fermion sign problem is also discussed.

Dirac fermions as a type of low-energy excitation quasiparticle widely exists in various condensed matter systems, such as the highly studied graphene, d-wave superconductors, and gapless semiconductors[1–5]. Due to the massless Dirac fermions having a linear dispersion relation and chiral symmetry, they usually exhibit singular and unconventional physical effects. For example, Dirac fermions can spontaneously open a gap through interacting, thus realizing a phase transition from a semimetal to an insulator or a superconductor[6]. The Gross-Neveu (GN) theory predicted that interacting Dirac fermions can be divided into three Wilson-Fisher universality classes: chiral Heisenberg, chiral Ising, and chiral XY[7–13]. The continuous phase transitions here usually go beyond the Landau paradigm[14–16]. A most famous example is the coupling between massless Dirac fermions and Ising fields in the form of chiral mass to produce chiral Ising universality class (or Gross-Neveu-Yukawa universality class)[17–21]. Recently, one of us discovered that a new chiral tricritical point emerged when coupling Dirac fermions to a tricritical Ising model[22]. The common but intriguing

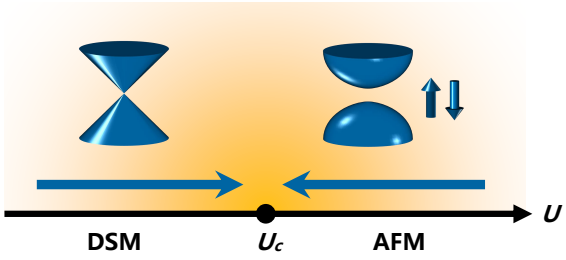

Figure 1. The schematic diagram of quenching from different initial states to the quantum critical point (QCP). The Hubbard interaction divides half-filled honeycomb fermions into Dirac semimetal phase (DSM) and antiferromagnetic phase (AFM). The yellow and pink in the figure represent different sublattices. The Dirac fermion in the left image is in momentum space, while the antiferromagnetic configuration in the right image is in real space. We prepared initial states of DSM and AFM respectively. These states were then quenched to the QCP in order to investigate their short-time relaxation dynamics.

quantum criticality territory of Dirac fermions may serve as a stepping stone towards more universal quantum phase transition picture.

Studying Dirac fermions presents a significant challenge for theoretical analysis due to the strong correlation. Non-perturbative numerical methods, such as determinant quantum Monte Carlo (DQMC), path integral molecular dynamics, can unbiasedly study the phase transition universal theory of interacting Dirac fermions[7,9,22–28]. In recent years, DQMC has gained popularity as a tool for investigating the ground-state characteristics of Dirac fermion systems. It has been successful in demonstrating equilibrium GN quantum criticality in these systems, although their results have not fully agreed with each other[29–34]. In addition, the non-equilibrium criticality of Dirac fermions often leads to new physics. For example, our previous renormalization group study found novel nonthermal fixed points in the Gross-Neveu-Yukawa system, as well as fermion-characteristic negative initial slip exponents around thermal fixed points. However, accurate numerical studies on GN quantum criticality are still lacking.

In terms of research methods, the typical approach to solving the ground-state fermions involves creating an initial trial wave function and then projecting it onto the ground state through imaginary-time evolution operators[35,36]. After a long period of imaginary time evolution, only information about the equilibrium ground state is obtained. However, they ignores important short-time information related to fermionic quantum criticality that is hidden in the initial state and imaginary time evolution process. According to dynamic scaling theory, this neglected short-time information not only sufficiently demonstrates all thermal criticalities of fermions but also includes nonequilibrium criticalities unique to short-time dynamics, such as memory effects on the initial state[26,37–44]. Moreover, nonequilibrium imaginary time dynamics can be observed in real-time dynamic experiments, and direct imaginary time dynamic experiments have already been preliminarily implemented in quantum computers[45–54].

Therefore, we are strongly motivated to develop numerical research on GN nonequilibrium quantum criticality, and this paradigm can be universally applied to the non-equilibrium dynamics of various fermion systems. This study for the first time extends DQMC for calculating fermionic nonequilibrium quantum criticality. We also demonstrated for the first time the nonequilibrium initial slip critical exponent of interacting Dirac fermions' chiral Heisenberg universality class. Specifically, we studied half-filled honeycomb Hubbard model with SU(2) symmetry at its critical point's imaginary time relaxation dynamics. The model is the most popular interacting Dirac fermion model but there was still no consensus on its phase transition behavior from previous equilibrium studies[9,25,29,34]. Unlike equilibrium methods where arbitrary trial wave functions are selected as initial states, we chose specific initial states and observed their imaginary time evolution processes at phase transition points instead of just studying ground states. With this nonequilibrium method that fully utilizes short-time information, we determined system's phase transition critical point and universal critical exponents with fewer computational resources while also calculating an initial slip exponent characterizing memory effects on the initial state. Finally, we mention potential applications of this method to address fermion sign problems.

Results

Model and protocol

We consider the two-dimensional spin-$\frac{1}{2}$ Hubbard model on a half-filled honeycomb lattice. The Hamiltonian reads

$$H = -t \sum_{\langle ij\rangle,\sigma} c^{\dagger}_{i\sigma} c_{j\sigma} + U \sum_{i} \left(n_{i\uparrow} - \frac{1}{2}\right)\left(n_{i\downarrow} - \frac{1}{2}\right), \quad (1)$$

in which $c^{\dagger}_{i\sigma}$ ($c_{j\sigma}$) represents the creation (annihilation) operator of spin $\sigma = \uparrow, \downarrow$ electrons, $n_{i\sigma} = c^{\dagger}_{i\sigma} c_{i\sigma}$ is the electron number operator on site i, and the summation index $\langle ij\rangle$ only sums over nearest neighbor sites. The coefficient t is the hopping amplitude, and U is the Coulomb repulsion potential. In the strong coupling limit $U/t \gg 1$ (weak coupling limit $U/t \ll 1$), the system tends to exhibit antiferromagnetic Mott insulator phase (Dirac semimetal phase)[34].

There exists a continuous phase transition critical point U_c/t between the two phases (Fig. 1), where the Hubbard interaction gives massless Dirac fermions an effective dynamic mass, leading to a transition from the Dirac semimetal phase (DSM) to the antiferromagnetic phase (AFM). Hereafter, we set $t = 1$ as the energy unit. In the strong coupling limit, this model can be map into a chiral Heisenberg model through Schrieffer-Wolff transformation[55]. The quantum criticality of chiral Heisenberg universality class play a role near this renormalization fixed point. The DSM-AFM transition here can be characterized by the antiferromagnetic order parame-

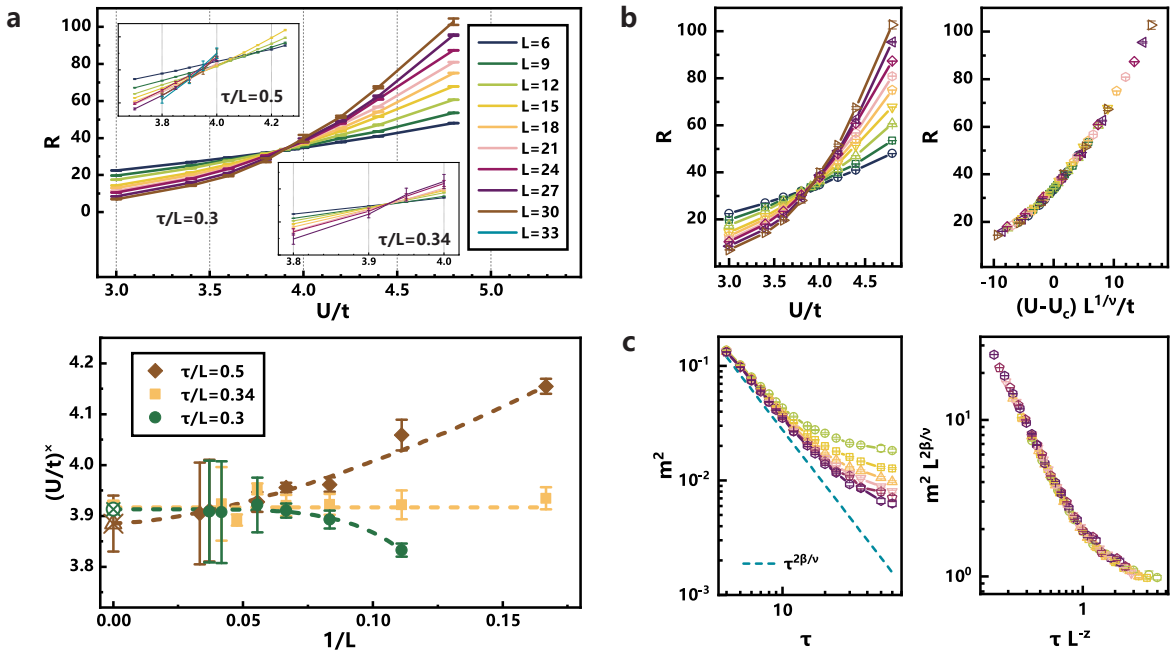

Figure 2. Relaxation dynamics with the AFM initial state. a Correlation ratio curves $R(U/t)$ of different sizes L intersect at the critical point. The upper figure shows the curves of $R(U/t)$ when $\tau/L = 0.3, 0.34, 0.5$ are fixed respectively. The lower figure extracts the intersection points $(U/c)^{\times}$ of adjacent size's $R(U/t)$ curves from the upper, and shows how these intersection points change with $1/L$. The critical point is extrapolated when the system tends to thermodynamic limit $L \to \infty$. The extrapolation result for $\tau/L = 0.3$ is $U/t = 3.91 \pm 0.03$, for $\tau/L = 0.34$ it is $U/t = 3.92 \pm 0.01$, and for $\tau/L = 0.5$ it is $U/t = 3.89 \pm 0.05$. Note that the extrapolation results are also marked at $1/L = 0$. **b** Correlation ratio at $\tau/L = 0.3$ and rescaling for phase transition parameter. The curves for different sizes are shown in different colors consistent with subfigure a. The left plot shows that the correlation ratios for different sizes do not overlap on both sides of the critical point. After rescaling the horizontal axis in the right plot, the curves for different sizes completely overlap, where $\nu = 1.17, U_c/t = 3.91$. **c** Relaxation curve and scaling of square of antiferromagnetic order parameter. Curves with size $L = 12 \sim 27$ are shown in different colors consistent with subfigure a. The left plot shows that m^2 exhibits power-law decay as $\tau^{2\beta/\nu}$ during short-time stage for large sizes. Here $\beta/\nu = 0.80$. In the right plot, after rescaling, curves for different sizes L perfectly overlap.

ter. We first define the antiferromagnetic structure factor[31,34]

$$S(\boldsymbol{q}) = \frac{1}{L^2} \sum_{i,j} e^{i\boldsymbol{q}\cdot(\boldsymbol{r}_i - \boldsymbol{r}_j)} \langle m_i^{(z)} m_j^{(z)} \rangle. \tag{2}$$

Here, staggered magnetization $m_i^{(z)}$ is defined as

$$m_i^{(z)} = \vec{c}_{i,A}^{\dagger} \sigma^z \vec{c}_{i,A} - \vec{c}_{i,B}^{\dagger} \sigma^z \vec{c}_{i,B}. \tag{3}$$

where i is the index of unit cell, A and B represent different sublattices, and Pauli-z matrix σ^z acting on the spin degree of freedom $\vec{c} = (c_\uparrow, c_\downarrow)$. Then, we calculate the square of AF order parameter as

$$m^2 = S(\boldsymbol{0}), \tag{4}$$

where $S(\boldsymbol{0})$ is the AF structure factor at zero momentum and is calculated by Eq. 2. In the following discussion, we denote the initial state's antiferromagnetic order parameter as m_0.

We employ the large-scale determinant quantum Monte Carlo (DQMC) method[36] to investigate the imaginary-time relaxation dynamics of our model. Due to the bipartite structure of honeycomb, there is no sign problem encountered during this process[56]. To approximate the quantum critical behavior at the thermodynamic limit, we conducted simulations on a lattice with periodic boundaries of limited size $L \times L$ cells. In Fig. 1, we illustrate that AFM, DSM, and spin random up-down state (RUD) were prepared as initial states for simulation of their imaginary-time evolution. We will demonstrate how short-time information can be utilized to determine the critical point and universal critical exponents below.

Antiferromagnetic ordered initial state

The saturated AFM initial state means that at the beginning of evolution, each electron occupies a lattice point on the honeycomb lattice, and the spin is arranged alternately up and down, with an order parameter $m_0 = 1$. At the critical point, fermionic fluctuations disrupt this ordered arrangement, causing the system to relax into DSM. Considering the ongoing controversy surrounding the determination of critical points based on equilibrium studies, we present short-time information to establish the critical point of phase transition. We define correlation ratio R as[31]

$$R = S(\boldsymbol{0}) / S(\Delta\boldsymbol{q}), \tag{5}$$

where $\Delta\boldsymbol{q} = \left(\frac{1}{L}\boldsymbol{b}_1 + \frac{1}{L}\boldsymbol{b}_2\right)$ is minimum lattice momentum. The correlation ratio is dimensionless. We set initial state to saturated AFM, and near the equilibrium critical point,

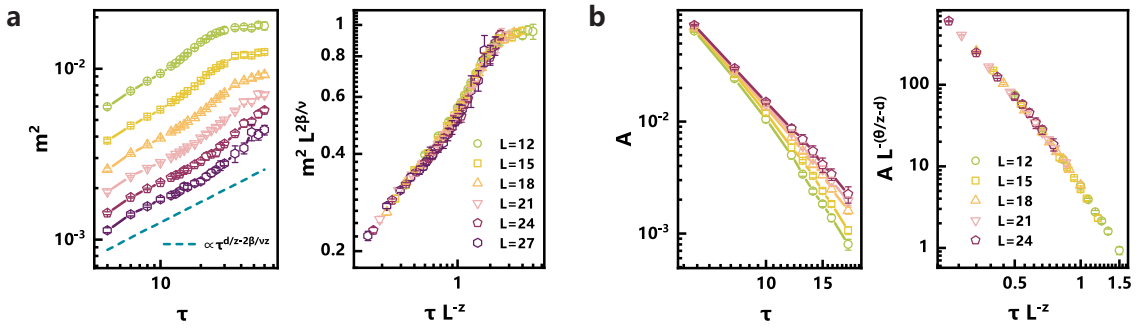

Figure 3. Relaxation dynamics with the disordered initial state. **a** Relaxation behavior of order parameter with the DSM initial state. The left plot shows that the order parameter for large size L increases in a form close to $\tau^{d/z-2\beta/\nu z}$. They have the same initial state $m_0 = 1$. The right plot has been rescaled on both axes, and curves of different sizes overlap. The critical exponent value chosen here is $\beta/nu = 0.80$. **b** Relaxation behavior of imaginary-time correlation with the RUD initial state. The left plot shows the relaxation curves of different sizes. The curves in the right plot are rescaled according to critical exponents $\theta = -0.84$, and the curves of different sizes overlap.

correlation ratio follows universal scaling form given by[38]

$$R(g,\tau,L) = f_R\left(gL^{1/\nu}, \tau^{-1}L^z\right), \tag{6}$$

where $g = (U - U_c)/t$ represents distance between system parameters and critical point. For Dirac fermions, dynamic critical exponent $z = 1$.

Here we fix $\tau^{-1}L^z$, so the correlation ratio at the critical point $g = 0$ is independent of size. As shown in Fig. 2a, we calculate the correlation ratio $R(U/t)$ as a function of Hubbard parameter for different sizes, and identify the intersection points $(U/c)^\times$ between curves for sizes L and $L+3$ as pseudo-critical points (PCP) for size L. We use an extrapolation form of $(U/c)^\times = a + bL^{-\omega}$ to obtain the thermodynamic limit value $U/t = 3.91 \pm 0.03$ of critical point at fixed $\tau/L = 0.3$. This result will be used in the following quantum criticality analysis, without loss of generality. The results with fixed values of $\tau/L = 0.34, 0.5$, also shown in Fig. 2a, extrapolate to the same critical point within error range, thus demonstrating that our method based on nonequilibrium information to determine critical points using dynamic scaling Eq. 5 is reliable.

The relaxation dynamics-based method we used above to solve the critical point can be applied universally to other fermion systems. Nevertheless, it is worth mentioning that as shown in Fig. 2a below, the PCP $(U/c)^\times$ approaches the critical point with different trends as L increases when different values of τ/L are taken. Specifically, when $\tau/L = 0.3$, the PCP under small size is smaller than the true critical point at thermodynamic limit; while when $\tau/L = 0.5$, the PCP under small size is larger than the true critical point; even more interestingly, we found that at $\tau/L = 0.34$, the PCP almost does not depend on size and can exhibit a real critical behavior under small sizes alone. This means that in the short-time stage, the PCP of the system tends to lean towards DSM, while after a long-time evolution, it leans towards AFM. This reversal of PCP shift has not been observed in previous phase transitions of bosonic systems and spin systems. Our preliminary understanding of this anomalous phenomenon is that during the short-time stage starting from antiferromagnetic state, fluctuations of Dirac fermions have a greater impact, while antiferromagnetic fluctuations dominate in the long time. Therefore, this phenomenon may be unique to critical points with these two degrees of freedom. This phenomenon may even suggest new methods for finding critical points through finite size-time effects by determining special moments like $\tau/L = 0.34$ based on judging trend of PCPs but further discussion will be omitted here. Additionally, this anomalous phenomenon caused by fermion fluctuations may provide important observable features for experiments.

According to the relaxation dynamics of correlation ratio, we can also determine the critical exponent ν of the correlation length. In previous numerical studies based on equilibrium states, there were significant differences in the numerical results for ν, and it was even uncertain whether it was greater than or less than 1[29,30,34]. We can measure the critical exponent ν in a short-time stage. Fixing $\tau/L = 0.3$, we obtain the universal scaling form of correlation ratio $R(g) = f_R\left(gL^{1/\nu}\right)$ from Eq. 6. It can be seen that curves of different sizes do not overlap on both sides of the phase transition point, as shown in Fig. 2b. We rescale the horizontal axis into $gL^{1/\nu}$ and adjust the value of ν so that curves of different sizes completely overlap, thereby fitting to obtain a critical exponent $\nu = 1.17 \pm 0.07$. Our result supports the research suggesting that $\nu > 1$[34]. The perfect rescaling shown in Fig. 2b also verifies both correctness and universality of Eq. 6, while testing accuracy our previously measured critical point $U_c/t = 3.91$ — if this is not accurate then it would be impossible to find a value for ν which makes curves with different sizes coincide.

After identifying the critical point, we can also use short-time dynamics to determine other critical exponents in a decisive manner. We take the order parameter critical exponent β as an example. The saturated AFM initialized relaxation

dynamics of the order parameter exhibit universal scaling

$$m^2 = \tau^{-2\beta/\nu z} f_{m^2}\left(\tau^{-1}L^z\right), \tag{7}$$

where f_{m^2} is a universal scaling function independent of system size. In Fig. 2c, we present relaxation behavior of $m^2(\tau)$ under different sizes and rescale them according to Eq. (7), fitting that all relaxation curves collapse into a universal functional form f_{m^2}. This yields a ratio between critical exponents $\beta/\nu = 0.80 \pm 0.03$. We verify the universality of our results by rescaling coincide in Fig. 2c. Combining with the previous measurement results of ν, we obtain the critical exponent of order parameter $\beta = 0.94 \pm 0.07$. This process can also be used to measure other critical exponents.

Disordered initial state

If we set the initial state into DSM, which is an eigenstate of the Hamiltonian with no interaction, then the initial state has no antiferromagnetic order. The universal scaling for the evolution of the order parameter at critical point $g = 0$ satisfies

$$m^2 = L^{-d}\tau^{d/z-2\beta/\nu z} f_{m^2}\left(\tau^{-1}L^z\right), \tag{8}$$

as shown in Fig. 3a. In short-time stage, $\tau^{-1}L^z$ in Eq. 8 is small enough that $f_{m^2}\left(\tau^{-1}L^z\right)$ can be approximated as a constant. Therefore, for a given size $m^2 \propto \tau^{d/z-2\beta/\nu z}$ and different sizes L, their relaxation curves do not overlap in short-time stage due to the factor of L^{-d} in proportionality coefficient, but they follow the same power law with increasing τ. As shown in Fig. 3a, different curves are approximately parallel with slope $d/z - 2\beta/\nu z$. Here we take finite size L as periodic boundary conditions relative to coarse-graining on momentum space's minimum distinguishable lattice. For larger sizes L, short-time scale represents longer timescale and range where order parameters grow according to power-law relation also increases accordingly. In thermodynamic limit $L \to \infty$, this range tends towards infinity; this is known as the critical slowing down. In this case, it becomes particularly important to use short-time methods to determine critical exponents. In addition, when $\tau = 0$, their initial state intercept follows a power law $m_0 \propto L^{-d}$. The Hamiltonian with no interaction can be directly diagonalized analytically to verify this relationship. In Fig. 3a, we also verified the critical exponent $\beta/\nu = 0.80$ obtained from the relaxation dynamics of AFM initial state. We rescaled the relaxation dynamics of DSM initial state using this result and found that curves of different sizes L overlap, which self-consistently confirms our results.

Another type of disordered initial state is RUD, which means that there is one electron on each lattice point, and their spins are randomly up or down without spatial correlation. The antiferromagnetic order parameter $m_0 = 0$ for this initial state. Here we can study the imaginary-time correlation. We define imaginary-time correlation as[41]

$$A = \frac{1}{L^2}\sum_i \langle m_i^{(z)}(0)\, m_i^{(z)}(\tau)\rangle, \tag{9}$$

where index i sums over all unit cells. $m_i^{(z)}(0)$ is a local staggered magnetization operator at initial time, which has the same dimension as the initial AF order parameter $m_0 \sim L^{-x_0}$. In a complete finite-size scaling analysis, Eq. 6, Eq. 7 and Eq. 8 should include dimensionless variable $m_0 L^{x_0}$, but our choice of initial state allows us to neglect this variable. According to definition Eq. 9 and $m_i \sim L^{-\beta/\nu}$, we can derive that A scales as $A \sim L^{x_0-\beta/\nu-d}$ where system dimension $d = 2$. Using scaling law[57]

$$x_0 = \theta z + \beta/\nu, \tag{10}$$

we obtain universal scaling

$$A = L^{\theta z-d} f_A\left(\tau^{-1}L^z\right). \tag{11}$$

The universality in this equation depends on critical point $g = 0$ and RUD initial state with disorder $m_0 = 0$. This means that besides Monte Carlo averaging, we also need to average over different samples of initial states numerically which greatly increases computational cost. Efficient nonequilibrium calculations enable us to obtain good results nonetheless. We show in Fig. 3b relaxation behavior of imaginary-time correlation $A(\tau)$, and control θ so that rescaled curves perfectly overlap in Eq. 11 form. From this, we determine the initial slip exponent $\theta = -0.84 \pm 0.04$, whose accuracy is verified by the overlap in Fig. 3b.

Thus, we for the first time determine the initial slip exponent θ of chiral Heisenberg universality class. This important critical exponent characterizes the memory of order parameter for the initial state, and has real-time observable effects[22,26,57–59]. It is worth noting that the initial slip exponent θ we obtained here is a negative value, which is consistent with the result we previously obtained using renormalization group in Gross-Neveu-Yukawa field theory[26]. This phenomenon is different from that of bosonic case. This suggests that during the short-time stage, large Dirac fermion fluctuations make the actual QCP larger than the mean-field critical point felt by electrons. This picture is consistent with our previous discussion of the short-time pseudo-critical point shifting towards disordered phase.

Discussion

In studying the nonequilibrium criticality of interacting fermions, we adopt a universal approach. This involves preparing specific initial states and simulating the system's imaginary-time evolution through DQMC. We then calculate observables based on equal-time Green's functions and study the scaling behavior of the system's relaxation dynamics. In this work, we demonstrate a specific methodology and results for applying this universal method to the interacting Dirac fermion system.

In our method, we do not need to go through a long wait until the system reaches equilibrium. We can obtain all critical exponents of the system and accurately predict its

Table 1. Quantum criticality of honeycomb Hubbard and chiral Heisenberg universality class. The first row of data in the table shows the numerical results obtained by our work through nonequilibrium fermion Monte Carlo methods. The remaining rows display related research findings for comparison purposes. In the table, honeycomb refers to the Hubbard model on a honeycomb lattice. It is important to note that our method is unique in its ability to calculate the nonequilibrium critical exponent θ.

model	method	U_c/t	ν	β	θ
honeycomb	QMC (present)	3.91(3)	1.17(7)	0.94(7)	−0.84(4)
honeycomb	QMC[34]	3.85(2)	1.02(1)	0.76(2)	-
honeycomb	QMC[29]	3.77(4)	0.84(4)	0.71(8)	-
Gross-Neveu	$4-\varepsilon$ (1st order)[9]	-	0.851	0.804	-
Gross-Neveu	$4-\varepsilon$ (2nd order)[9]	-	1.01	0.995	-
Gross-Neveu	FRG[25]	-	1.31	1.32	-

critical behavior in equilibrium state through a short imaginary time evolution process. The introduction of this method may significantly improve the efficiency of numerical studies on fermions and save computational resources. For the Hubbard model in honeycomb lattice, we compare our results with previous research results in Table 1. Considering that there is still no consensus on the critical point and critical exponents of this model in past results, our results can also serve as a new reference.

Moreover, this work opens up a universal path for studying nonequilibrium criticality in interacting fermionic systems. By controlling the given initial state, our method can investigate the influence of the initial state on imaginary time evolution. We have determined the initial slip exponent for chiral Heisenberg universality class in interacting fermionic systems to be $\theta = -0.84 \pm 0.04$. These achievements fill the gap in research on non-equilibrium criticality of fermionic quantum systems.

Furtherly, our nonequilibrium approach has the potential to address the challenging fermion sign problem, which has hindered progress in numerically studying fermionic systems[19,28,60]. This problem arises during simulations of imaginary-time evolution of fermions and can result in negative weights in Monte Carlo sampling, rendering importance sampling ineffective. However, our method requires only a short imaginary time evolution to predict critical behavior of the system, potentially enabling us to overcome this limitation. Our future work will focus on exploring this direction.

Methods

Imaginary-time dynamics

Our research on relaxation dynamics is based on imaginary time evolution[38]. Considering the Wick rotation $t \to \mathrm{i}\tau$, the equation of motion for imaginary time dynamics is the imaginary-time Schrödinger equation

$$\frac{\partial}{\partial \tau}|\psi(\tau)\rangle = H|\psi(\tau)\rangle. \tag{12}$$

This evolution is not unitary, so we use a normalized formal solution

$$|\psi(\tau)\rangle = Z_0^{-1} \mathrm{e}^{\tau H}|\psi(0)\rangle, \tag{13}$$

where the modulus $Z_0 = \left\| \mathrm{e}^{\tau H}|\psi(0)\rangle \right\|$ has been normalized out. The imaginary time evolution operator $\mathrm{e}^{\tau H}$ projects the initial state $|\psi(0)\rangle$ onto its energy ground state $|E_0\rangle$, i.e.,

$$\begin{aligned} |\psi(\tau)\rangle &= Z_0^{-1} \sum_n \mathrm{e}^{\tau E}|E_n\rangle \langle E_n|\psi(0)\rangle \\ &\sim |E_0\rangle + c_1 \mathrm{e}^{\tau\Delta}|E_1\rangle \end{aligned} \tag{14}$$

where $|E_n\rangle$ represents the n-th excited state, $\Delta = E_1 - E_0$ is the energy gap between the first excited state and the ground state, and c_1 is a constant. Here we only consider the first excited state because higher-energy excitations decay much faster than the first. For finite gap Δ, after long-time evolution, the wave function $|\psi(\tau)\rangle$ is completely projected onto the ground state without any information about excited states. We are interested in short-time dynamics before reaching to this ground state with relaxation time scale of $\zeta \sim \frac{1}{\Delta}$. At critical points where energy gap closes ($\Delta \to 0$), relaxation process becomes infinitely slow showing critical slowing down.

Determinant quantum Monte Carlo

We employ the large-scale determinant quantum Monte Carlo (DQMC) method[36,61–63] to investigate the imaginary-time relaxation dynamics of our model. Specifically, we prepare a specific initial state $|\psi_0\rangle$ and set the system parameters U/t on the critical point to observe the scaling behavior of observables during the short-time stage. When the system evolves to imaginary time τ (less than relaxation time ζ), the expectation value of observables is given by

$$\langle O(\tau)\rangle = \frac{\langle\psi_0|\mathrm{e}^{\tau H/2} O \mathrm{e}^{\tau H/2}|\psi_0\rangle}{\langle\psi_0|\mathrm{e}^{\tau H}|\psi_0\rangle}. \tag{15}$$

In numerical calculations, we use Trotter decomposition[64] to discretize imaginary-time propagator into $M = \tau/\Delta\tau$ (M is integer) time slices with

$$\mathrm{e}^{\tau H} = \left(\mathrm{e}^{\Delta\tau H_t}\mathrm{e}^{\Delta\tau H_U} + \mathscr{O}\left(\Delta\tau^2\right)\right)^M, \tag{16}$$

where H_t and H_U are the hopping term and Hubbard interaction term respectively in the Hamiltonian (Eq. 1). We choose small enough $\Delta\tau/t < 0.05$. To decouple two-body

fermion-fermion coupling form of $e^{\Delta\tau H_U}$, we use a discrete Hubbard-Stratonovich transformation

$$e^{-\frac{\Delta\tau U}{2}\left(n_{i\uparrow}+n_{i\downarrow}\right)^2} = \sum_{l=\pm1,\pm2} \gamma(l) e^{i\sqrt{\frac{\Delta\tau U}{2}}\eta(l)\left(n_{i\uparrow}+n_{i\downarrow}\right)} \quad (17)$$

to obtain one-body fermion-auxiliary field coupling. Here, we introduce a four-component space-time local auxiliary fields[65] $\gamma(\pm1) = 1+\sqrt{6}/3, \gamma(\pm2) = 1-\sqrt{6}/3$, $\eta(\pm1) = \pm\sqrt{2\left(3-\sqrt{6}\right)}, \eta(\pm2) = \pm\sqrt{2\left(3+\sqrt{6}\right)}$, and use DQMC for importance sampling over these space-time configurations. More details used here are similar to those employed when solving thermal ground states as described in Ref.[36]. Due to the bipartite structure of honeycomb, there is no sign problem encountered during this process[56].

References

1. Novoselov, K. S. *et al.* Electric field effect in atomically thin carbon films. *science* **306**, 666–669 (2004).
2. Zhang, Y., Tan, Y.-W., Stormer, H. L. & Kim, P. Experimental observation of the quantum hall effect and berry's phase in graphene. *nature* **438**, 201–204 (2005).
3. Hasan, M. Z. & Kane, C. L. Colloquium: topological insulators. *Rev. modern physics* **82**, 3045 (2010).
4. Murakami, S. Phase transition between the quantum spin hall and insulator phases in 3d: emergence of a topological gapless phase. *New J. Phys.* **9**, 356, DOI: 10.1088/1367-2630/9/9/356 (2007).
5. Tsuei, C. C. & Kirtley, J. R. Pairing symmetry in cuprate superconductors. *Rev. Mod. Phys.* **72**, 969–1016, DOI: 10.1103/RevModPhys.72.969 (2000).
6. Boyack, R., Yerzhakov, H. & Maciejko, J. Quantum phase transitions in Dirac fermion systems. *The Eur. Phys. J. Special Top.* **230**, 979–992, DOI: 10.1140/epjs/s11734-021-00069-1 (2021).
7. Gross, D. J. & Neveu, A. Dynamical symmetry breaking in asymptotically free field theories. *Phys. Rev. D* **10**, 3235 (1974).
8. Wilson, K. G. & Fisher, M. E. Critical exponents in 3.99 dimensions. *Phys. Rev. Lett.* **28**, 240–243, DOI: 10.1103/PhysRevLett.28.240 (1972).
9. Rosenstein, B., Hoi-Lai Yu & Kovner, A. Critical exponents of new universality classes. *Phys. Lett. B* **314**, 381–386, DOI: https://doi.org/10.1016/0370-2693(93)91253-J (1993).
10. Gies, H. & Wetterich, C. Renormalization flow of bound fermion states. *Phys. Rev. D* **71**, 095006, DOI: 10.1103/PhysRevD.71.095006 (2005).
11. Herbut, I. F. Interacting electrons in graphene: Fermi velocity renormalization and effective four-fermion interaction. *Phys. Rev. B* **79**, 085116, DOI: 10.1103/PhysRevB.79.085116 (2009).
12. Nambu, Y. & Jona-Lasinio, G. Dynamical model of elementary particles based on an analogy with superconductivity. i. *Phys. Rev.* **122**, 345–358, DOI: 10.1103/PhysRev.122.345 (1961).
13. Nambu, Y. & Jona-Lasinio, G. Dynamical model of elementary particles based on an analogy with superconductivity. ii. *Phys. Rev.* **124**, 246–254, DOI: 10.1103/PhysRev.124.246 (1961).
14. Yu, X.-J., Pan, Z., Xu, L. & Li, Z.-X. Non-Hermitian strongly interacting Dirac fermions: a quantum Monte-Carlo study (2023). ArXiv:2302.10115 [cond-mat, physics:quant-ph].
15. Bi, Z., Lake, E. & Senthil, T. Landau ordering phase transitions beyond the landau paradigm. *Phys. Rev. Res.* **2**, 023031, DOI: 10.1103/PhysRevResearch.2.023031 (2020).
16. Sachdev, S. & Yin, X. Quantum phase transitions beyond the landau–ginzburg paradigm and supersymmetry. *Annals Phys.* **325**, 2–15, DOI: 10.1016/j.aop.2009.08.003 (2010).
17. Zinn-Justin, J. *Quantum field theory and critical phenomena*, vol. 171 (Oxford university press, 2021).
18. Wang, T.-T. & Meng, Z. Y. Emus live on the gross-neveu-yukawa archipelago (2023). 2304.00034.
19. Li, Z.-X., Jiang, Y.-F. & Yao, H. Fermion-sign-free Majarana-quantum-Monte-Carlo studies of quantum critical phenomena of Dirac fermions in two dimensions. *New J. Phys.* **17**, 085003, DOI: 10.1088/1367-2630/17/8/085003 (2015).
20. Jiang, Y.-F., Li, Z.-X., Kivelson, S. A. & Yao, H. Charge-4*e* superconductors: A majorana quantum monte carlo study. *Phys. Rev. B* **95**, 241103, DOI: 10.1103/PhysRevB.95.241103 (2017).
21. Li, Z.-X., Jiang, Y.-F. & Yao, H. Solving the fermion sign problem in quantum monte carlo simulations by majorana representation. *Phys. Rev. B* **91**, 241117, DOI: 10.1103/PhysRevB.91.241117 (2015).
22. Yin, S., Jian, S.-K. & Yao, H. Chiral Tricritical Point: A New Universality Class in Dirac Systems. *Phys. Rev. Lett.* **120**, 215702, DOI: 10.1103/PhysRevLett.120.215702 (2018).
23. Wilson, K. G. The renormalization group: Critical phenomena and the kondo problem. *Rev. Mod. Phys.* **47**, 773–840, DOI: 10.1103/RevModPhys.47.773 (1975).
24. Polchinski, J. Effective field theory and the fermi surface. *arXiv preprint hep-th/9210046* (1992).
25. Janssen, L. & Herbut, I. F. Antiferromagnetic critical point on graphene's honeycomb lattice: A functional renormalization group approach. *Phys. Rev. B* **89**, 205403, DOI: 10.1103/PhysRevB.89.205403 (2014).
26. Jian, S.-K., Yin, S. & Swingle, B. Universal Prethermal Dynamics in Gross-Neveu-Yukawa Criticality. *Phys. Rev.*

Lett. **123**, 170606, DOI: 10.1103/PhysRevLett.123.170606 (2019).

27. Xiong, Y. & Xiong, H. Path-integral molecular dynamics for anyons, bosons, and fermions. *Phys. Rev. E* **106**, 025309, DOI: 10.1103/PhysRevE.106.025309 (2022).

28. Xiong, Y. & Xiong, H. On the thermodynamic properties of fictitious identical particles and the application to fermion sign problem. *The J. Chem. Phys.* **157**, 094112, DOI: 10.1063/5.0106067 (2022).

29. Assaad, F. F., Parisen Toldin, F., Hohenadler, M. & Herbut, I. F. Fermionic quantum criticality in honeycomb and π-flux Hubbard models: Finite-size scaling of renormalization-group-invariant observables from quantum Monte Carlo. *Phys. Rev. B* **91**, 165108, DOI: 10.1103/PhysRevB.91.165108 (2015).

30. Assaad, F. F. & Herbut, I. F. Pinning the Order: The Nature of Quantum Criticality in the Hubbard Model on Honeycomb Lattice. *Phys. Rev. X* **3**, 031010, DOI: 10.1103/PhysRevX.3.031010 (2013).

31. Sorella, S., Otsuka, Y., Seki, K. & Yunoki, S. Dirac electrons in the square lattice Hubbard model with a d-wave pairing field: chiral Heisenberg universality class revisited. *Phys. Rev. B* **102**, 235105, DOI: 10.1103/PhysRevB.102.235105 (2020). ArXiv:2009.04685 [cond-mat].

32. Sorella, S., Seki, K., Otsuka, Y. & Yunoki, S. Fermi-liquid ground state of interacting Dirac fermions in two dimensions. *Phys. Rev. B* **99**, 125145, DOI: 10.1103/PhysRevB.99.125145 (2019).

33. Sorella, S., Otsuka, Y., Seki, K. & Yunoki, S. Quantum criticality in the metal-superconductor transition of interacting Dirac fermions on a triangular lattice. *Phys. Rev. B* **98**, 035126, DOI: 10.1103/PhysRevB.98.035126 (2018).

34. Sorella, S., Otsuka, Y. & Yunoki, S. Universal quantum criticality in the metal-insulator transition of two-dimensional interacting Dirac electrons. *Phys. Rev. X* **6**, 011029, DOI: 10.1103/PhysRevX.6.011029 (2016). ArXiv:1510.08593 [cond-mat, physics:hep-lat].

35. Da Liao, Y., Xu, X. Y., Meng, Z. Y. & Qi, Y. Dirac fermions with plaquette interactions. II. SU(4) phase diagram with Gross-Neveu criticality and quantum spin liquid. *Phys. Rev. B* **106**, 115149, DOI: 10.1103/PhysRevB.106.115149 (2022). ArXiv:2205.07173 [cond-mat].

36. Assaad, F. F. Quantum monte carlo methods on lattices: The determinantal approach. *Quantum Simulations Complex Many-Body Syst. From Theory to Algorithms* **10**, 99–147 (2002).

37. Yin, S., Huang, G.-Y., Lo, C.-Y. & Chen, P. Kibble-Zurek Scaling in the Yang-Lee Edge Singularity. *Phys. Rev. Lett.* **118**, 065701, DOI: 10.1103/PhysRevLett.118.065701 (2017).

38. Yin, S., Mai, P. & Zhong, F. Universal short-time quantum critical dynamics in imaginary time. *Phys. Rev. B* **89**, 144115, DOI: 10.1103/PhysRevB.89.144115 (2014).

39. Shu, Y.-R., Jian, S.-K. & Yin, S. Nonequilibrium Dynamics of Deconfined Quantum Critical Point in Imaginary Time. *Phys. Rev. Lett.* **128**, 020601, DOI: 10.1103/PhysRevLett.128.020601 (2022).

40. Zhang, S., Yin, S. & Zhong, F. Generalized dynamic scaling for quantum critical relaxation in imaginary time. *Phys. Rev. E* **90**, 042104, DOI: 10.1103/PhysRevE.90.042104 (2014).

41. Shu, Y.-R. & Yin, S. Short-imaginary-time quantum critical dynamics in the j-q 3 spin chain. *Phys. Rev. B* **102**, 104425, DOI: 10.1103/PhysRevB.102.104425 (2020).

42. Huang, R.-Z. & Yin, S. Kibble-Zurek mechanism for a one-dimensional incarnation of a deconfined quantum critical point. *Phys. Rev. Res.* **2**, 023175, DOI: 10.1103/PhysRevResearch.2.023175 (2020).

43. Hohenberg, P. C. & Halperin, B. I. Theory of dynamic critical phenomena. *Rev. Mod. Phys.* **49**, 435–479, DOI: 10.1103/RevModPhys.49.435 (1977).

44. Li, Z.-X., Yin, S. & Shu, Y.-R. Imaginary-time quantum relaxation critical dynamics with semi-ordered initial states. *Chin. Phys. Lett.* **40**, 037501, DOI: 10.1088/0256-307X/40/3/037501 (2023).

45. Liu, S., Zhang, S.-X., Hsieh, C.-Y., Zhang, S. & Yao, H. Probing many-body localization by excited-state variational quantum eigensolver. *Phys. Rev. B* **107**, 024204, DOI: 10.1103/PhysRevB.107.024204 (2023).

46. Bernien, H. *et al.* Probing many-body dynamics on a 51-atom quantum simulator. *Nature* **551**, 579–584, DOI: 10.1038/nature24622 (2017).

47. Peotta, S., Brange, F., Deger, A., Ojanen, T. & Flindt, C. Determination of dynamical quantum phase transitions in strongly correlated many-body systems using loschmidt cumulants. *Phys. Rev. X* **11**, 041018, DOI: 10.1103/PhysRevX.11.041018 (2021).

48. Sun, S.-N. *et al.* Quantum computation of finite-temperature static and dynamical properties of spin systems using quantum imaginary time evolution. *PRX Quantum* **2**, 010317, DOI: 10.1103/PRXQuantum.2.010317 (2021).

49. Janković, V. & Vučičević, J. Fermionic-propagator and alternating-basis quantum monte carlo methods for correlated electrons on a lattice. *The J. Chem. Phys.* **158**, 044108, DOI: 10.1063/5.0133597 (2023).

50. Motta, M. *et al.* Determining eigenstates and thermal states on a quantum computer using quantum imaginary time evolution. *Nat. Phys.* **16**, 205–210, DOI: 10.1038/s41567-019-0704-4 (2020).

51. Nishi, H., Kosugi, T. & Matsushita, Y.-i. Implementation of quantum imaginary-time evolution method on nisq devices by introducing nonlocal approximation. *npj Quantum Inf.* **7**, 85, DOI: 10.1038/s41534-021-00409-y (2021).

52. Tarruell, L., Greif, D., Uehlinger, T., Jotzu, G. & Esslinger, T. Creating, moving and merging dirac points with a fermi gas in a tunable honeycomb lattice. *Nature* **483**, 302–305, DOI: 10.1038/nature10871 (2012).

53. Greif, D., Jotzu, G., Messer, M., Desbuquois, R. & Esslinger, T. Formation and dynamics of antiferromagnetic correlations in tunable optical lattices. *Phys. Rev. Lett.* **115**, 260401, DOI: 10.1103/PhysRevLett.115.260401 (2015).

54. Prüfer, M. *et al.* Observation of universal dynamics in a spinor Bose gas far from equilibrium. *Nature* **563**, 217–220, DOI: 10.1038/s41586-018-0659-0 (2018).

55. Schrieffer, J. R. & Wolff, P. A. Relation between the anderson and kondo hamiltonians. *Phys. Rev.* **149**, 491–492, DOI: 10.1103/PhysRev.149.491 (1966).

56. Sorella, S. & Tosatti, E. Semi-metal-insulator transition of the hubbard model in the honeycomb lattice. *Europhys. Lett.* **19**, 699, DOI: 10.1209/0295-5075/19/8/007 (1992).

57. Janssen, H. K., Schaub, B. & Schmittmann, B. New universal short-time scaling behaviour of critical relaxation processes. *Zeitschrift für Physik B Condens. Matter* **73**, 539–549, DOI: 10.1007/BF01319383 (1989).

58. Shu, Y.-R., Yin, S. & Yao, D.-X. Universal short-time quantum critical dynamics of finite-size systems. *Phys. Rev. B* **96**, 094304, DOI: 10.1103/PhysRevB.96.094304 (2017).

59. Li, Z., Schülke, L. & Zheng, B. Finite-size scaling and critical exponents in critical relaxation. *Phys. Rev. E* **53**, 2940–2948, DOI: 10.1103/PhysRevE.53.2940 (1996).

60. Troyer, M. & Wiese, U.-J. Computational complexity and fundamental limitations to fermionic quantum monte carlo simulations. *Phys. Rev. Lett.* **94**, 170201, DOI: 10.1103/PhysRevLett.94.170201 (2005).

61. Blankenbecler, R., Scalapino, D. J. & Sugar, R. L. Monte carlo calculations of coupled boson-fermion systems. i. *Phys. Rev. D* **24**, 2278–2286, DOI: 10.1103/PhysRevD.24.2278 (1981).

62. Hirsch, J. E. Two-dimensional hubbard model: Numerical simulation study. *Phys. Rev. B* **31**, 4403–4419, DOI: 10.1103/PhysRevB.31.4403 (1985).

63. Assaad, F. & Evertz, H. World-line and determinantal quantum monte carlo methods for spins, phonons and electrons. In *Computational Many-Particle Physics*, 277–356, DOI: 10.1007/978-3-540-74686-7_10 (Springer Berlin Heidelberg, Berlin, Heidelberg, 2008).

64. Hatano, N. & Suzuki, M. *Finding Exponential Product Formulas of Higher Orders*, 37–68 (Springer Berlin Heidelberg, Berlin, Heidelberg, 2005).

65. Assaad, F. F., Imada, M. & Scalapino, D. J. Charge and spin structures of a $d_{x^2-y^2}$ superconductor in the proximity of an antiferromagnetic mott insulator. *Phys. Rev. B* **56**, 15001–15014, DOI: 10.1103/PhysRevB.56.15001 (1997).

Acknowledgements

This work is supported by (national) college students innovation and entrepreneurship training program, Sun Yat-sen University.

Author Contributions

S.Y. and Z.-X.L. conceived the research idea. Z.-X.L provided guidance on the basic framework of Monte Carlo simulations and algorithms. Y.-K.Y. conducted Monte Carlo simulations, processed data, and wrote the manuscript. Z.Z. and Y.-K.Y polished algorithms and debugged programs. S.Y. and Y.-K.Y analyzed short-time dynamics. S.Y. providing guidance on nonequilibrium scaling theory.

Competing interests

The authors declare no competing interests.